Science of the Total Environment 705 (2020) 135868

Contents lists available at ScienceDirect

Science of the Total Environment

journal homepage: www.elsevier.com/locate/scitotenv

Quantifying the response of potential flooding risk to urban growth in Beijing

Yibing Wang [a,b], Xianhong Xie [a,b,*], Shunlin Liang [c], Bowen Zhu [a,b], Yi Yao [a,b], Shanshan Meng [a,b], Chuiyu Lu [d]

[a] State Key Laboratory of Remote Sensing Science, Jointly Sponsored by Beijing Normal University and Institute of Remote Sensing and Digital Earth of Chinese Academy of Sciences, Beijing 100875, China
[b] Beijing Engineering Research Center for Global Land Remote Sensing Products, Institute of Remote Sensing Science and Engineering, Faculty of Geographical Science, Beijing Normal University, Beijing 100875, China
[c] Department of Geographical Sciences, University of Maryland, College Park, USA
[d] China Institute of Water Resources and Hydropower Research, State Key Laboratory of Simulation and Regulation of Water Cycle in River Basin, Beijing 100038, China

HIGHLIGHTS

- Urban growth in Beijing was monitored from 1980 to 2015 based on Landsat data.
- Surface runoff yields were identified using a land-surface hydrological model.
- The impervious surface fraction increased from 8.73% in 1980 to 22.22% in 2015.
- The simulated runoff coefficient in 2010 was approximately doubled compared to 1980.
- The impervious surface fraction of 6% is the detectable threshold in response to potential flooding risk.

GRAPHICAL ABSTRACT

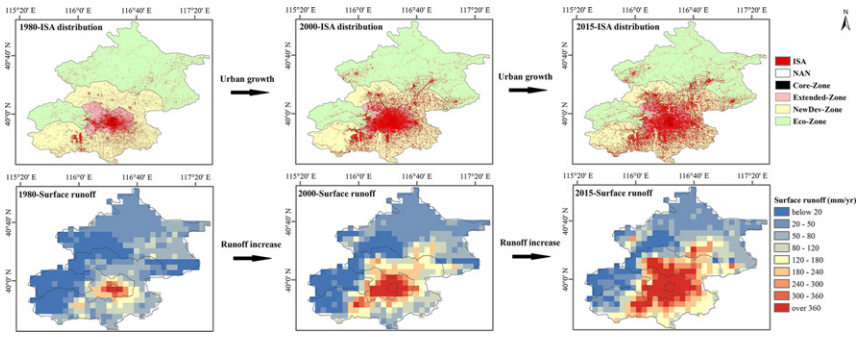

ARTICLE INFO

Article history:
Received 2 October 2019
Received in revised form 28 November 2019
Accepted 28 November 2019
Available online 2 December 2019

Editor: Damia Barcelo

Keywords:
Landsat data
Impervious surface
Surface runoff
Potential flooding risk
Beijing
Land surface hydrological modeling

ABSTRACT

Global urban growth leads to a great increase in the impervious surface area (ISA) such as roads, plazas, airports, and parking lots, and consequently reshapes hydrological regimes in urban basins. Beijing, the capital of China, has experienced rapid urban growth since the 1980s. However, the spatial-temporal variability of the ISA and its impact on flooding risk are unclear. This study monitored urban growth (i.e., the evolution of the ISA) in Beijing for the period of 1980–2015 based on Landsat data, and identified the response of surface runoff yield using a land-surface hydrological model. The modeling at a relatively high spatial resolution (~6 km) was driven with retrieved long-term ISA dynamics, Global LAnd Surface Satellite (GLASS) product, and climate forcings. The results show that the impervious surface fraction (ISF) in Beijing increased from 8.73% (1448.16 km^2) in 1980 to 22.22% (3685.92 km^2) in 2015. With a demarcation at around the year 2000, the ISA growth presents a new pattern with a northeast-southwest direction from the Core Functional Zone (Core-Zone). Due to the ISA expansion, the simulated runoff coefficient in 2010 is approximately doubled compared to that of 1980. We identified an ISF threshold of approximately 6%, beyond which every 1% increase in the ISF may increase the surface runoff by approximately 5.51 mm/year, and thereby poses a high potential flooding risk even under a moderate rainfall event. In four typical historical storms, the sensitivity coefficients of surface runoff to precipitation and ISF were 0.97 and 0.63, respectively, indicating impervious surfaces dramatically enhanced the potential flooding risk. Our findings have implications for urban planning and the construction of sponge city in Beijing.

* Corresponding author at: Beijing Normal University, China.
E-mail addresses: ybwang@mail.bnu.edu.cn (Y. Wang), xianhong@bnu.edu.cn (X. Xie).

https://doi.org/10.1016/j.scitotenv.2019.135868
0048-9697/

1. Introduction

Global urban growth is illustrated by the fact that over 55% of the 7.6 billion people on earth currently live in cities and metropolitan areas, up from 5% in 1900 (UN, 2018). This dramatic demographic shift has accompanied land conversion, typically from natural and cropland to artificial surfaces with relatively low permeability (Rose and Peters, 2001; Yang et al., 2011; Zhou et al., 2013). The artificial surfaces include roads, plazas, airports, parking lots, and roofs, which are generally referred to as the impervious surface area (ISA). Land conversion that causes disrespects to land capability with environmental land use conflicts, e.g., ISA expansion, can generally influence the intensity of processes such as infiltration and runoff (Caldas et al., 2018). Specifically, precipitation on ISA can be converted directly into surface runoff within a short time and generate runoff and routing (Fletcher et al., 2013; Konrad and Booth, 2005; Milly et al., 2008), consequently decreasing evapotranspiration and baseflow and increasing surface runoff and flooding risk (Olang and Fürst, 2011; Yang et al., 2010). Therefore, high-density ISA within an extreme weather event has been assumed to exacerbate casualties and property damage (Jha et al., 2012; Jiang et al., 2018). For example, Beijing, as the capital of China, has experienced rapid population and construction space expansion since 1978 (Statistics, 2018). As evidenced by a 3000-year record, it is an area vulnerable to flooding due to the climate conditions and environmental factors (Xie et al., 2019).

Techniques to minimize flooding risk in urban areas have also been promoted in many studies, such as rainwater harvesting, discharge detention, and "sponge city" related measures. Rainwater harvesting and discharge detention are complementary measures to attenuate peak flows and to improve water productivity for basic human needs and other productive activities (Bellu et al., 2016; Sanches Fernandes et al., 2015; Terêncio et al., 2017). The "sponge city" for stormwater management was proposed in China to rationally manage the urban layout and improve water infiltration and storage using permeable materials. Currently, this program has been applied in many cities including megacities of Beijing, Tianjin, Shanghai, and Shenzhen (Chan et al., 2018; Jiang et al., 2018; Xu et al., 2017). Undoubtedly, the implementation of these Technologies relies heavily on knowledge of hydrological responses to urban growth (Xia et al., 2017).

To understand the role of urban growth on the potential flooding risk in Beijing, two questions should arise. First, what has been the urban dynamic in Beijing during past decades? The urban dynamic in this study is defined as the spatial-temporal distribution of ISAs. Remote sensing is a useful technique to address this question as it provides data to monitor land use/land cover change at various spatial and temporal scales. Especially, Landsat data (including Thematic Mapper [TM]; Enhanced Thematic Mapper plus [ETM+]; Operational Land Imager [OLI]) have been widely used because of the availability of long-term data (Banskota et al., 2014). For example, Landsat data were used to map human settlement changes in China (Gong et al., 2019), the change of ISA in the Washington, D.C.–Baltimore, MD metropolitan (Sexton et al., 2013), and the urban transitions of the Red River Delta in Vietnam (Miguel et al., 2014; Yang et al., 2010). Li et al. (2015) derived the annual urban dynamics of Beijing based on Landsat data and indicated the importance of mapping the long-term ISA of Beijing.

Second, what is the evolution of surface runoff yield in response to urban growth? This question could be addressed based on water discharge observations with long-term series and storm event-based data (Miller et al., 2014). However, the data are usually sparse and therefore limit such studies. Alternatively, hydrological models are widely used because they are able to simulate hydrological processes across various scales so as to compensate for the inadequacy of observations, and to design different scenarios for purposeful analysis and projections (Yang et al., 2011). Therefore, hydrological modeling is preferred in urban flood detection (Salvadore et al., 2015). For example, the Variable Infiltration Capacity (VIC) model (Liang et al., 1994; Liang et al., 1996) was successfully used to identify the runoff response to urban intensity in the White River Basin, Indiana (Yang et al., 2011; Yang et al., 2010). For more cases of hydrological modeling, please refer to Pumo et al. (2017) and Salvadore et al. (2015) where relatively comprehensive reviews were given regarding the applications of hydrological models in urban watersheds.

With the availability of urban dynamic data, it is essential to incorporate this information into hydrological modeling. Currently, however, most studies using hydrological modeling have only considered two or three scenarios regarding pre-urbanization and post-urbanization conditions, thereby quantifying the contribution of urban growth to the hydrological cycle in urban watersheds (Yang et al., 2010; Zhou et al., 2013). Urban growth is generally a continuous process along with ISA increase, therefore, hydrological modeling should reflect the urban dynamics and other land cover changes to conduct a reasonable simulation with respect to runoff generation and flood risk analysis (Pumo et al., 2017).

The objective of this study is to identify the response of annual surface runoff yields and flood events to urban growth in Beijing. The ISA maps of Beijing were first extracted based on Landsat data thereby detecting the urban growth pattern during the period of 1980–2015. A land-surface hydrological model, i.e., the VIC model, was employed at a spatial resolution of 0.0625° (~6 km). The feature of the hydrological modeling is that the ISA dynamics and vegetation parameters from satellite remote sensing products are incorporated in the modeling. It should be noted that we focused on spatial-temporal surface runoff depth analysis over Beijing for the annual surface runoff yields and flood events, which is assumed to represent the potential flooding risk rather than the real flooding or waterlogging conditions. The findings of this study are expected to be valuable for understanding the interaction between impervious surfaces and hydrological processes, and give implications for flood mitigation measures (e.g., the sponge city program) and urban planning in megacities worldwide like Beijing.

2. Study area and data

2.1. Study area

Beijing is located in northern China and has an area of nearly 16,584 km^2 (Fig. 1). The northwest region is surrounded by mountains which cover 62% of the total area. It had over 21 million permanent residents in 2018, compared to 9 million in 1980. The construction and completed floor space was approximately 696.63 km^2 in 2018, which had increased by 28.61 times compared to the area in 1980 (23.525 km^2) (Statistics, 2018). According to the Eleventh Five-Year Plan, Beijing is divided into four functional zones: the Core Functional Zone (Core-Zone, 94 km^2, 0.57%), the Urban Functional Extended Zone (Extended-Zone, 1289 km^2, 7.77%), the New Urban Development Zone (NewDev-Zone, 6322 km^2, 38.12%), and the Ecological Conservation Zone (Eco-Zone, 8880 km^2, 53.54%). The Core-Zone is used to develop political and cultural distinctions (e.g., historic buildings, conference centers), the Extended-Zone and the NewDev-Zone focus on the development of commerce and manufacturing, respectively, and the Eco-Zone serves as a green ecological barrier and provides protection for water sources. Thus, the ISAs are mainly distributed in the first three zones.

Beijing has a warm monsoon climate which is characterized by large seasonal variations in temperature and precipitation. The annual temperature ranges from 6 to 14 °C with a northwest-southeast increasing gradient. Annual precipitation is approximately 500 mm during the period 1975–2015 (Fig. 1). Precipitation is mainly affected by topography and the monsoon climate, resulting in an extremely uneven seasonal distribution of precipitation, with 80% concentrated in summer when the city is seriously susceptible to flooding. Under such climate conditions and land surface transformation, flooding has increasingly become a devastating disaster in Beijing (Jia et al., 2019). It has experienced over

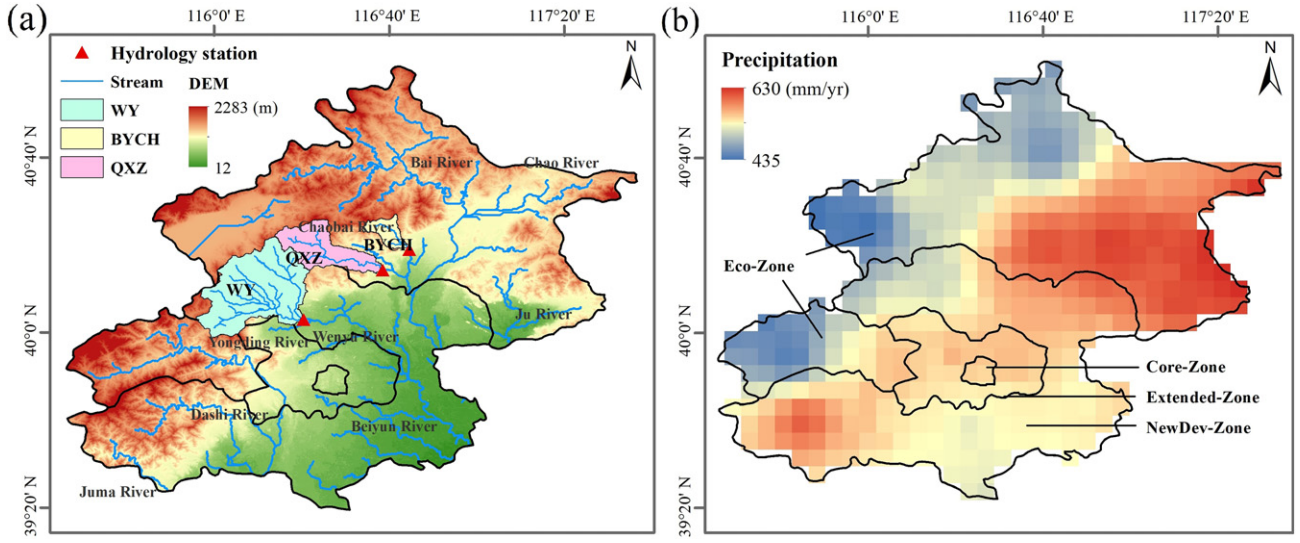

Fig. 1. Information of Beijing: (a) location of Beijing and three hydrological stations: Wenyu (WY), Boyachang (BYCH), Qianxinzhuang (QXZ), with the digital elevation model (DEM) as the background; (b) distribution of annual precipitation and four function zones from 1975 to 2015.

40 extreme climate and flooding events since 2004 (Yang et al., 2016). A typical example was the July 21, 2012 flooding event which caused 70 deaths and the facility paralysis, with economic losses of approximately 16 billion RMB (Xu, 2018).

2.2. Data

2.2.1. Data for ISA extraction

In this study, we refer to the ISA definition given by Liu et al. (2011): sites that are dominated by human activities and habitation through the construction of transportation and buildings, including all anthropogenic materials that water cannot infiltrate (e.g., roads, buildings, and square). "Dominated" indicates >50% coverage with built environments within each pixel. Landsat remote sensing data (obtained from United States Geological Survey [USGS], http://earthexplorer.usgs.gov/) were used to extract the ISA. Since Beijing covers two remote sensing tiles, we downloaded two image tiles every five years from 1980 to 2015, thus, a total of 16 tiles of images were employed to extract the ISA. The quality of Landsat images was first manually examined to select cloud-free images and to minimize the time difference between two tiles of images during the same time period. Data for 1980 was derived from Landsat-MSS, with a spatial resolution of 78 m, and other data were derived from Landsat-TM and Landsat-OLI with a spatial resolution of 30 m. All images were processed to L2T-level (e.g., passed the corrections of topography and radiation) and were geometrically registered with geometric errors of less than one pixel. The nearest neighbor resampling technique was used to resample the Landsat images into a pixel size of 30 m during image-to-image registration.

These Landsat images were then inlaid into eight sets for the years 1980, 1985, 1990, 1995, 2000, 2005, 2010, and 2015 using the Classification Regression Tree (CART) method for ISA extraction. The CART method will be described in Section 3.1.

2.2.2. Data for hydrological model input

The VIC model input included topographical, meteorological forcing, soil, and vegetation data. The topographical (i.e., the digital elevation model; DEM) data was obtained from USGS with 90 m resolution. The DEM was used to delineate river networks and extract watersheds that were necessary for runoff routing. The meteorological forcing variables used in this study included precipitation, maximum and minimum air temperature, and wind speed. The daily data regarding these variables were from Zhu et al. (2019) with a spatial resolution of 0.0625° (~6 km). The data were produced by interpolating observations from meteorological stations and have been evaluated over China with encouraging reliability (Xie et al., 2015; Zhu et al., 2019). The soil dataset that was used to define the VIC model parameters was obtained based on a 30 × 30 arc-second-resolution soil characteristics dataset (Zhu et al., 2019). In this dataset, soil physical parameters such as field capacity, wilting point, saturated hydraulic conductivity, and bulk density were derived based on a China soil dataset (Dai et al., 2013; Wei et al., 2013). The other parameters (e.g., bubbling pressure, thermal damping depth) were defined according to the soil dataset from Food and Agriculture Organization (FAO) (Nijssen et al., 2001).

The land use changes in the period of 1980–2015 were represented with eight land cover maps which were created by merging Landsat TM digital images (Liu et al., 2014; Liu et al., 2003; Liu et al., 2010) with a spatial resolution of 1 km (referred to as base maps of land cover). However, this land cover dataset may render substantial bias for the spatial-temporal distribution of ISAs due to the coarse resolution (Gong et al., 2019; Xie et al., 2015). Therefore, the land use type of urban region in these base maps were replaced by our new ISA extraction.

This study produced new ISA maps for Beijing with a spatial resolution of 30 m based on the data described in Section 2.2.1. Thus, the base maps (i.e., the base maps of land cover) were overlaid with the new ISA maps to achieve new land cover maps which were used in the VIC modeling. Moreover, the leaf area index (LAI), as an important parameter of vegetation condition, was calculated using the Global Land Surface Satellite (GLASS) product and was incorporated in the modeling (Liang et al., 2013; Liang et al., 2014). The GLASS LAI data set were derived from multi-satellite reflectance using general regression neural networks at 8-day temporal resolution and 1-km spatial resolution from 1981 to 2018 (Xiao et al., 2014; Xiao et al., 2016). Other vegetation parameters were extracted from Zhu et al. (2019). Therefore, eight sets of vegetation parameters were prepared corresponding to land cover maps to capture vegetation dynamics in Beijing.

2.2.3. Data for model evaluation

Three stations of streamflow data were available from the Annual Hydrological Report for the P.R. China (AHR, 2016). As shown in Fig. 1, the three stations (i.e., Boyachang [BYCH], Qianxinzhuang [QXZ], and Wenyu [WY]), are located at the outlets of three catchments with drainage areas of 98, 344, and 859 km^2, respectively. The data from the three stations were separated into calibration and validation periods for the VIC evaluation. Streamflow observations were converted to runoff by dividing the area of the corresponding watershed so that the simulated runoff could be compared with the observations at monthly or yearly

scales. The three catchments can be viewed as representative since they have various land cover types, including ISAs, crop, forest, and grass. Based on the similarity of land cover and soil properties, the VIC parameters could be transferred from gauged catchments to ungauged areas based on the land cover distribution.

3. Methods

The workflow of this study can be divided into three parts as shown in Fig. 2: ISA extraction and data preparation, hydrological model setup and evaluation, and scenario design and potential flood risk analysis. The methods associated with the first two are described subsequently in this section. The results of the third part are presented in Section 4.

3.1. ISA extraction

The CART method was applied to obtain the ISA distribution in Beijing based on Landsat images. The CART is a decision tree method which divides training samples into uniform subsets using a recursive binary segmentation approach (Zhang and Qian, 2015). The tree structure (e.g., branches and nodes) was established when dividing training samples and was applied to the subsequent image classification (Wu et al., 2012). Due to its flexibility and capability, CART has been widely used in many studies and serves as a standard method in the USGS Geological Analysis and Monitoring Plan for the national land cover database (Qi and Yue, 2011).

The classification process was divided into three steps. First, each Landsat image was divided into nine categories (water body, bare land, cropland, square, roads, forest, grass, old buildings, and new buildings) using the CART method. Second, the filter-merge method was used to eliminate mutation points (e.g., building grids surrounded by water bodies) from appearing in the classification results. Third, the improved results were binarized to extract the ISA distribution based on the infiltration properties of the nine categories; buildings, square, and roads were classified as ISA, and the other categories were considered permeable surface area.

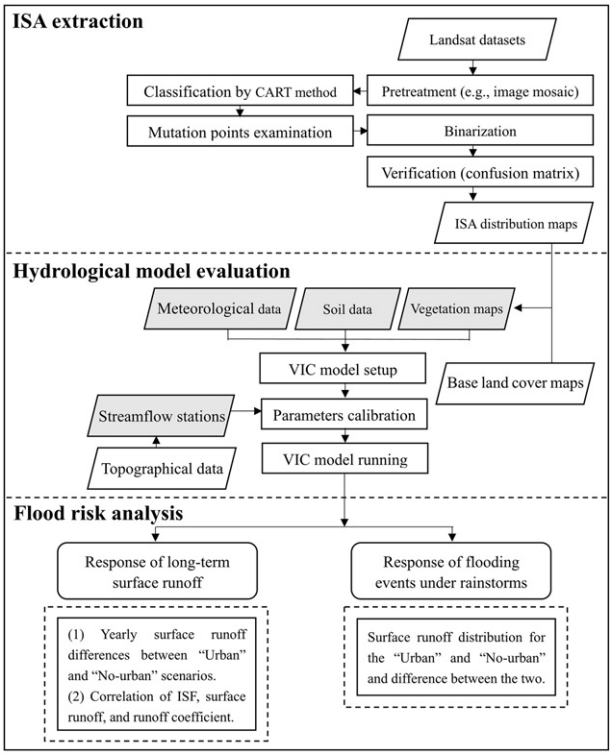

Fig. 2. The workflow of this work.

The classification verification process was also divided into three steps. First, we generated 200 testing samples from the entire image using a random sampling method. Second, the testing samples were manually classified into impervious or permeable types by referring to the high-resolution image (e.g., Google Earth). The first and second steps were repeated until 150 testing samples were obtained for each impervious and permeable type, thus the testing samples were basically consistent with a random distribution. Then, the testing samples were used to establish a confusion matrix to value the accuracy of the classification in the third step. The confusion matrix included the product's accuracy (PA), the user's accuracy (UA), the overall accuracy (OA), and the kappa coefficient (Table 1). Please note that we repeated the selection of testing samples for each classification result (i.e., each image) because of the dynamic changes in land cover.

3.2. The VIC model development and its setup

As a large-scale land-surface hydrological model, the VIC model was used in this study as it has been successfully applied in studies on various scales (Cuo et al., 2013; Liang and Xie, 2001; Nijssen et al., 2001; Xie et al., 2015; Xie et al., 2007). Among many land surface hydrological models, the VIC model is distinguished by its variable infiltration curve and a nonlinear relationship between baseflow and deep soil moisture (Liang et al., 1994; Liang et al., 1996). It divides a study area into grids, and represents multiple vegetation types and one main soil layer within each grid cell, which is regarded as an independent unit for a simulation. Moreover, it can simulate water and energy balance from the land surface to the soil profile (Liang and Xie, 2001; Xie et al., 2003). The VIC model was therefore employed to quantify the hydrologic response to urban growth in Beijing.

The VIC model was run with a resolution of 0.0625° (~6 km) and a daily time step, which was consistent with the resolution of the meteorological forcing data. Its parameters should be calibrated to improve the streamflow simulation and reflect the impact of land cover in Beijing (Lohmann et al., 1998; Nijssen et al., 2003). Although the VIC model parameters have been well verified over China by Zhu et al. (2019), we further calibrated seven empirical and influential parameters for Beijing using streamflow observations. The seven parameters included the infiltration parameter (B), the three baseflow parameters (D_S, D_m, and W_S), and the thicknesses of three soil layers. For more detailed information about these parameters please refer to Liang et al. (1994), Liang et al. (1996), and Liang and Xie (2001). The model calibration was conducted to adjust the seven model parameters so as to match the runoff simulations with the observations. The calibrated model parameters were then transferred to ungauged basins in Beijing based on similarities of soil and land cover.

The VIC model does not have a specific module to consider hydrological processes in urban areas. Therefore, to reflect the low permeability of the land cover with ISA, we modified the VIC program code. Rainfall on the ISA was assumed to directly become surface runoff. This treatment was set according to Yang et al. (2010), as it is considered suitable in urbanized regions.

To explore the urban growth effect on surface runoff generation during the period of 1980–2015, we performed two simulation scenarios with VIC modeling. One involved simulating the real hydrological processes under urban growth and is referred to as an "Urban" scenario. In this scenario, the land cover information (i.e., the land cover maps merged the base maps of land cover with the new ISA maps, as described in Sections 2.2.2 and 3.1) in VIC was updated every five years, i.e., at the beginning of 1980, 1985, 1990, 1995, 2000, 2005, and 2010. The land cover map for 2015 was not used in the modeling because the map of 2010 was used to represent the land cover conditions for the period of 2010–2015. Through the period of 1980–2015, there were seven sets of vegetation parameters based on the related land cover maps that were described in Sections 2.2.1 and 3.1. Please note

Table 1
Confusion matrix and decision parameters for ISA extraction results.

		Non-ISA	ISA	UA (%)			Non-ISA	ISA	UA (%)
	Non-ISA	**138**	14	91%		Non-ISA	**146**	13	92%
1980	ISA	12	**136**	92%	**2000**	ISA	4	**137**	97%
	PA (%)	92%	91%	**91%**		PA (%)	97%	91%	**94%**
		Kappa = 0.83					**Kappa = 0.89**		
		Non-ISA	ISA	UA (%)			Non-ISA	ISA	UA (%)
	Non-ISA	**142**	19	88%		Non-ISA	**141**	17	89%
1985	ISA	8	**131**	94%	**2005**	ISA	9	**133**	94%
	PA (%)	95%	87%	**91%**		PA (%)	94%	89%	**91%**
		Kappa = 0.82					**Kappa = 0.83**		
		Non-ISA	ISA	UA (%)			Non-ISA	ISA	UA (%)
	Non-ISA	**144**	17	89%		Non-ISA	**135**	14	91%
1990	ISA	6	**133**	96%	**2010**	ISA	15	**136**	90%
	PA (%)	96%	89%	**92%**		PA (%)	90%	91%	**90%**
		Kappa = 0.85					**Kappa = 0.81**		
		Non-ISA	ISA	UA (%)			Non-ISA	ISA	UA (%)
	Non-ISA	**148**	14	91%		Non-ISA	**137**	9	94%
1995	ISA	2	**136**	99%	**2015**	ISA	13	**141**	92%
	PA (%)	99%	91%	**95%**		PA (%)	91%	94%	**93%**
		Kappa = 0.89					**Kappa = 0.85**		

that this "Urban" scenario was the simulation that underwent calibration and validation as described in Section 4.2.

The second scenario was based on a synthetic condition in which we assumed no urban growth in Beijing, and is denoted as the "No-urban" scenario. The modeling was only fed with the land cover map of 1980 and the land cover and vegetation parameters were not updated through the 1980–2015 period. Therefore, the simulated results from the "Urban" scenario can be viewed as the combined effect of climate change and urban growth, and the results from the "No-urban" scenario are only contributed by climate change. Under the first-order approximation, the simulation difference between the two scenarios is assumed to represent the hydrological effect of urban growth.

3.3. Evaluation index

In the evaluation, several measures were used to quantitatively evaluate the performance of the model and the impact of the impervious surface fraction (ISF) on surface runoff. Three statistical indices, Nash–Sutcliffe efficiency (*NSE*) (Nash and Sutcliffe, 1970), relative error (E_r), and correlation coefficient (R) were used to describe the agreements between the simulated and observed data, and R was also used to track the relative relationship associated with the surface runoff and ISF. These indexes are defined as follows:

$$NSE = 1 - \frac{\sum_{i=1}^{n}\left(Q_{obs,i} - Q_{sim,i}\right)^2}{\sum_{i=1}^{n}\left(Q_{obs,i} - \overline{Q}_{obs}\right)^2} \quad (1)$$

$$E_r = \frac{\bar{Q}_{sim} - \bar{Q}_{obs}}{\bar{Q}_{obs}} \times 100\% \quad (2)$$

$$R = \frac{\sum_{i=1}^{n}\left(Q_{obs,i} - \overline{Q}_{obs}\right)\left(Q_{sim,i} - \overline{Q}_{sim}\right)}{\sqrt{\sum_{i=1}^{n}\left(Q_{obs,i} - \overline{Q}_{obs}\right)^2}\sqrt{\sum_{i=1}^{n}\left(Q_{sim,i} - \overline{Q}_{sim}\right)^2}} \quad (3)$$

where $Q_{obs,\,i}$ is the observed streamflow for a month (year) i, $Q_{sim,\,i}$ is the simulated streamflow for a month (year) i, the $\overline{Q}_{sim}$ and $\overline{Q}_{obs}$ are simulated and observed mean runoff during the whole period, respectively.

A sensitivity coefficient (S_c) was adopted to identify the sensitivity of surface runoff to changes in precipitation or ISF, as it is a partial derivative based algorithm (Beven, 1979). Its non-dimensional form is expressed as (Hao et al., 2018):

$$S_c = \lim_{X \to 0} \frac{\Delta Q / Q}{\Delta X / X} \quad (4)$$

where X is the factor that affects surface runoff (Q), referring to the ISF or precipitation in this study. A positive (or negative) S_c means that surface runoff will be enhanced (or shrunk) as the X increase. For the sensitivity to precipitation, the change of Q (ΔQ) was calculated based on the "No-urban" scenario; for the sensitivity to ISF, ΔQ was described as the difference of Q between the "Urban" scenario and the "No-urban" scenario.

4. Results

4.1. Urban growth

We first evaluated the accuracy of the ISA extraction. As presented in Table 1, the OAs of all Landsat scenes exceeded 90%, and the kappa coefficients were higher than 0.8, which indicated that

the classification results were generally credible. The varied accuracies among the scenes were largely associated with image quality, including their acquisition dates, cloud coverage, or variations in climatic conditions.

The ISA had a significant upward trend over Beijing. As shown in Fig. 3, the ISAs increased from 1448.16 km^2 around 1980 to 3685.92 km^2 around 2015, with an increasing linear trend of approximately 48.11 km^2/year. The increase primarily occurred in the Extended-Zone and the NewDev-Zone, where the ISF increased by approximately 33% and 21%, respectively. Small changes occurred in the Core-Zone after the ISF increased from approximately 81% to 91% during 1980–1985, and the ISF in the Eco-Zone remained below 8%. In the period of 1980–2000, the ISA growth was mainly concentrated in the Core-Zone and the Extended-Zone. After 2000, the ISAs spread to the NewDev-Zone with a southwest-northeast direction.

We integrated the eight ISA distributions with the corresponding base land cover maps to discuss the land use transformation. Fig. 4 presents the land use for 1980 and 2015. The Extended-Zone and the NewDev-Zone had the largest land use change among the four zones. The most obvious change was the conversion from dry crop land (e.g., corn/wheat) to ISA, followed by wet cropland (e.g., paddy field) conversion to ISA, the two land use types decreased by 51.12% and 33.79% respectively. Other land use types, such as woodland and water bodies, were mainly affected by the environment and topography, and changed by <8% over the three and a half decades.

4.2. Hydrological model evaluation

The VIC model was calibrated and validated using the streamflow data from the three watersheds. Table 2 and Fig. 5 show the model performance for the calibration and validation periods. The VIC simulations agreed well with the runoff observations as they showed similar patterns for the temporal dynamics for both the calibration and validation periods. Particularly, the simulations had an encouraging feature in their ability to capture high-flow dynamics.

For the calibration period, the *NSEs* in three stations were >0.4, and *R* was >0.8. However, the monthly runoff for the QXZH and the BYC watersheds was overestimated with E_rs of approximately 47.36% and 11.66%, respectively, especially for the low-flow process estimation. This overestimation is probably attributable to the fact that the VIC modeling designed in this study failed to consider other human activities on hydrological processes. For example, the modeling did not consider water resources allocations for industrial uses which may impose a substantial impact on the streamflow.

For the validation period, the *NSEs* for three stations were >0.7, with *R* >0.8. Similarly as in the calibration period, the monthly runoff for the QXZH and the BYC watersheds was overestimated with E_rs of approximately 54.94% and 22.42%, respectively, and the yearly runoff for the WY watershed was overestimated with E_r of approximately 9.05%. The larger E_r compared to the calibration period may be due to the increased intensity of human activities. Despite the overestimation, the VIC model demonstrated an acceptable performance for the runoff simulation after model

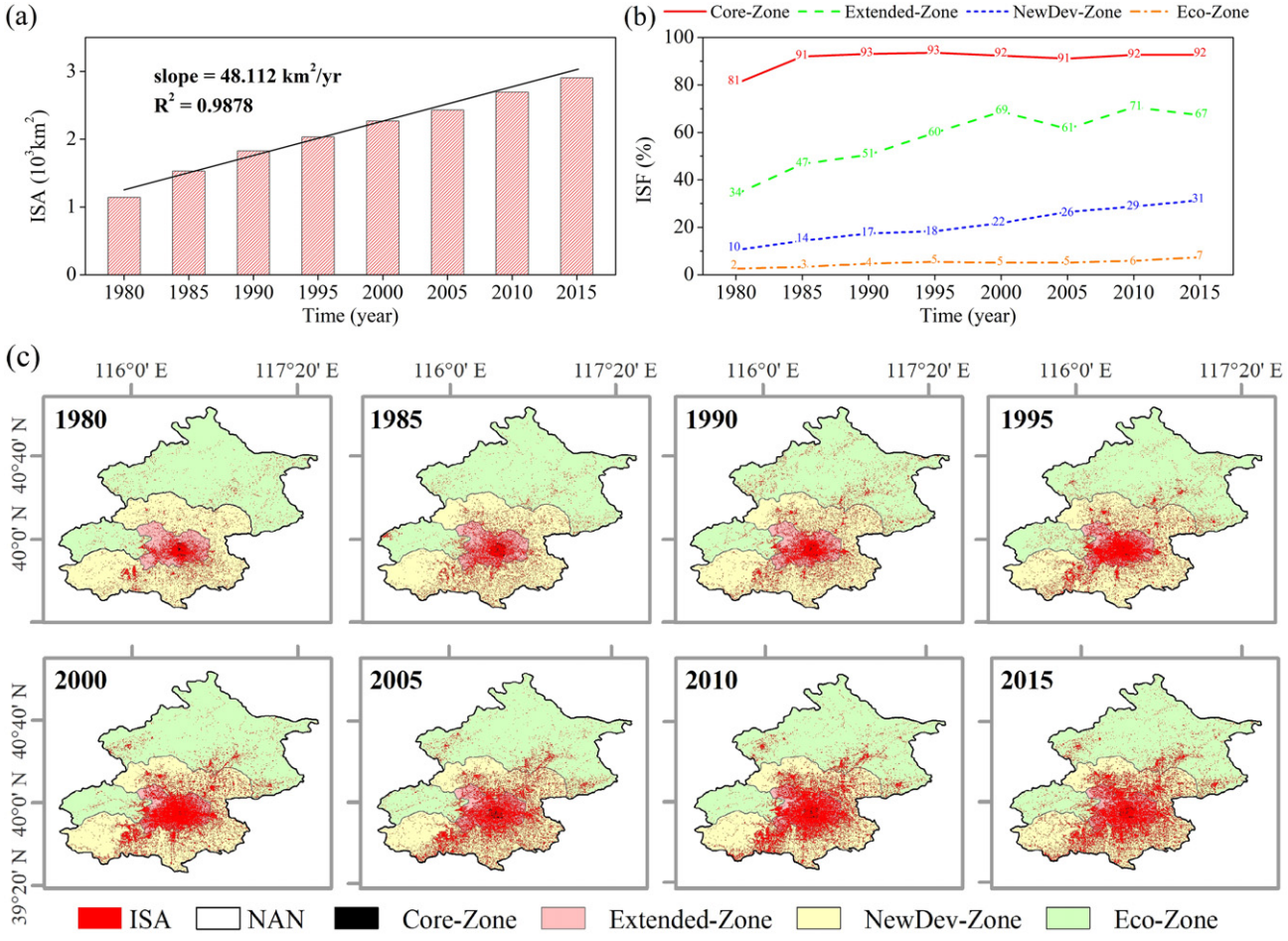

Fig. 3. Temporal-spatial variation of ISA in Beijing: (a) Temporal variation of ISA; (b) temporal variation of ISF in Beijing and the four zones; (c) ISA distribution maps, with four zones shown in different colors as background.

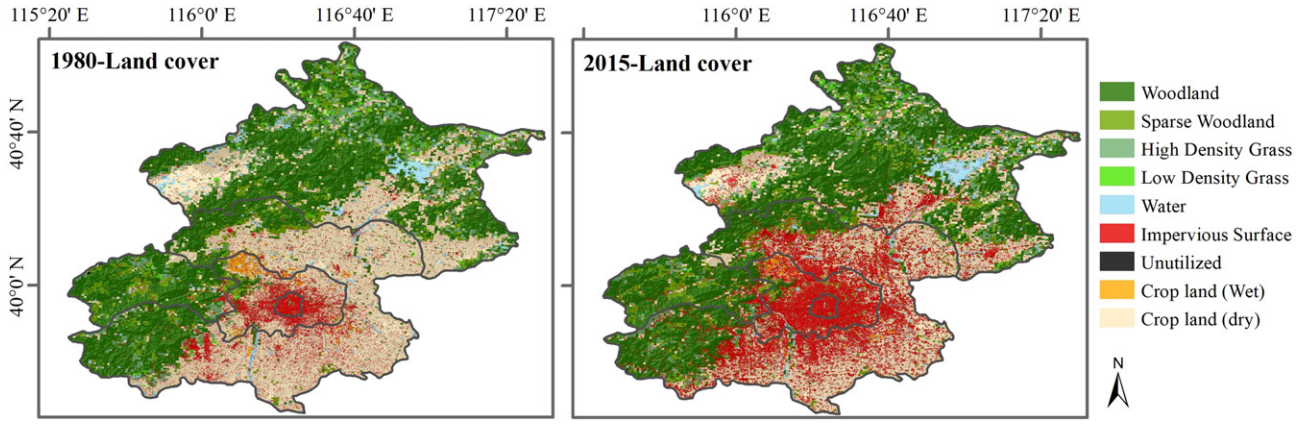

Fig. 4. The land cover types of Beijing in 1980 (left) and 2015 (right), respectively.

calibration. Therefore, the VIC model and the parameter values can be used to identify the hydrological effect of the ISA expansion in Beijing.

4.3. Response of surface runoff to urban growth

After model evaluation, the simulated results based on the "Urban" and "No-urban" scenarios were used to identify the impact of urban growth. As shown in Fig. 6, annual surface runoff increased in the four zones during the period of 1980–2015, and especially in the Extended-Zone where the annual surface runoff was approximately 156.2 mm during 1980–1984 and increased to 415.5 mm during 2010–2014. When comparing the results from the "Urban" and the "No-urban" scenarios, the increased surface runoff was primarily attributable to the ISA expansion, which contributed the largest surface runoff increase in the Extended-Zone (5.50 mm/year), followed by the NewDev-Zone (3.04 mm/year), the Core-Zone (1.23 mm/year), and the Eco-Zone (0.50 mm/year).

Along with the increasing surface runoff, the surface runoff coefficient (RC) presented a similar pattern (Fig. 7). Overall, the RC of Beijing increased from 0.12 in 1980–1984 to 0.25 in 2010–2014. The Extended-Zone had the highest increase from 0.36 to 0.71 for the same periods. Moreover, the Core-Zone exhibited the largest RC (mean of 0.9), and the Eco-Zone had the lowest mean RC of 0.10.

The spatial distributions of surface runoff and RC were consistent with the ISF variability. Fig. 8 presents the spatial distributions of mean surface runoff and RC, together with the ISF for four five-year representative periods in every decade. During the past 36 years, the high density of ISA (ISF > 70%) spread from the Core-Zone to the Extended-Zone. The number of grid cells with ISF > 70% increased from 6 during 1980–1984 to 34 during 2010–2014. Under such urban growth, high annual surface runoff and RC also extended from the Core-Zone to the Extended-Zone. In the whole of Beijing, annual surface runoff was approximately 70.4 mm during 1980–1984, and 135.9 mm during 2010–2014.

To roughly quantify the consequence of urban growth, we calculated the R for the surface runoff/RC and ISF, which provides a measure of how closely surface runoff generation and ISF rankings are in agreement. As shown in Fig. 8, the annual surface runoff had a high correlation with the ISF ($R = 0.6$) for the four representative periods. The R between annual surface runoff and ISF increased with the ISF, and reached 0.74 during 2010–2014. A similar pattern also appeared for R between the RC and the ISF.

Owing to the high spatial correlation described above, we further detected the relationship between the surface runoff generation and ISF. For the period of 2010–2014, we plotted the mean annual surface runoff against the associated ISF for each grid cell, and the variation of daily surface runoff, which was represented by the standard deviation of daily surface runoff for 2010–2014. As shown in Fig. 9, interestingly,

Table 2
Model performance for the three watersheds.

Station	Calibration			Validation		
	NSE	E_r	*R*	*NSE*	E_r	*R*
QXZH	0.46	47.36%	0.84	0.72	54.94%	0.93
BYC	0.66	11.66%	0.84	0.72	22.42%	0.87
WY	0.59	−0.18%	0.83	0.86	9.05%	0.99

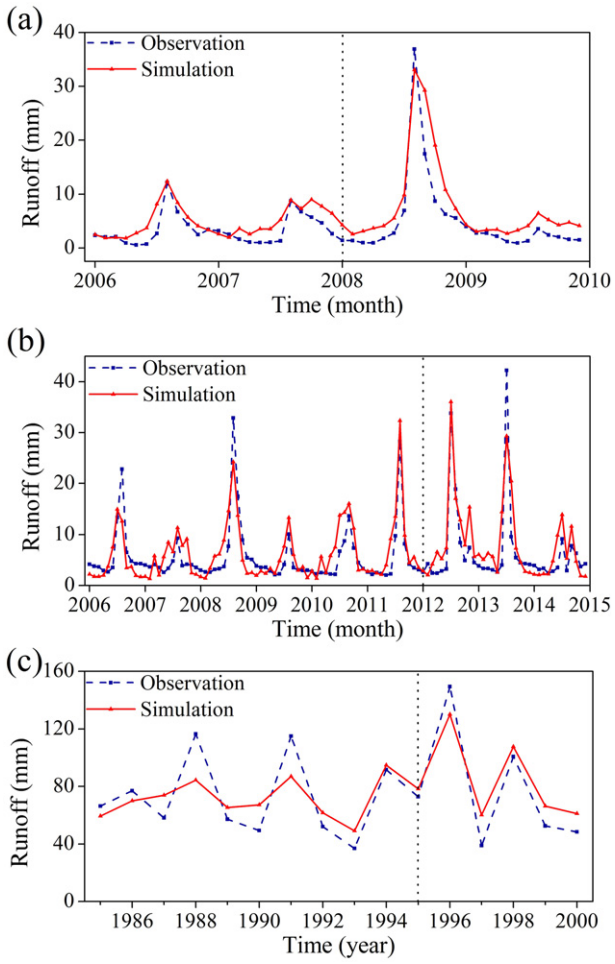

Fig. 5. Simulated discharge compared to observations: (a) QXZ; (b) BYCH; and (c) WY. The dark dotted line divides the data for calibration period (before) and validation period (after).

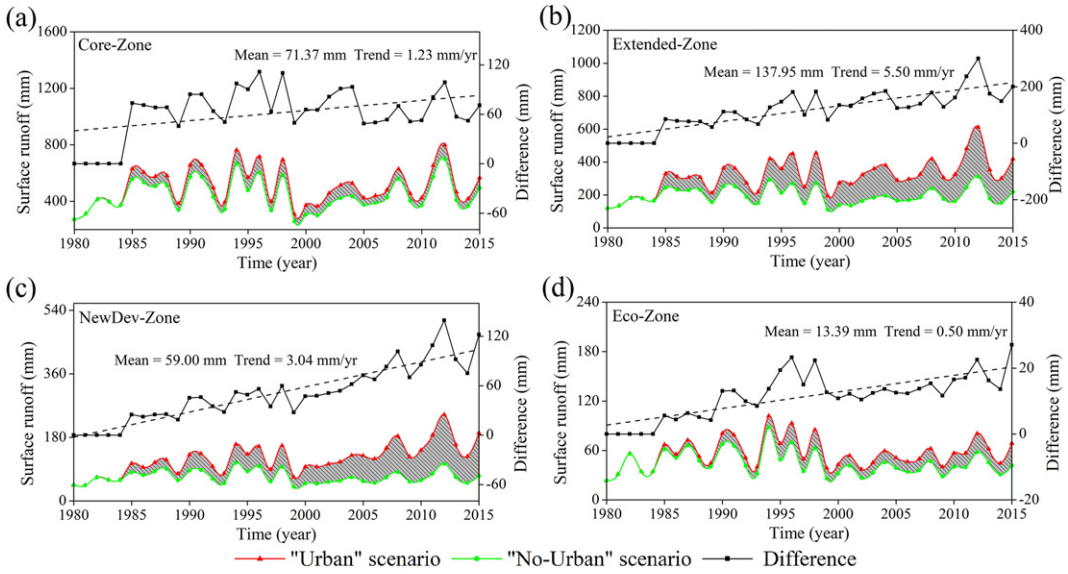

Fig. 6. The yearly surface runoff and its differences of "Urban" and "No-urban" scenario in the four zones: (a) Core-Zone; (b) Extended-Zone; (c) NewDev-Zone; and (d) Eco-Zone. The shaded area represents the difference between the two scenarios.

the annual surface runoff had a strong linear correlation with the ISF if the ISF was >6%. A 1% rise of ISF may cause an increase in the annual surface runoff of 5.51 mm. Moreover, the standard deviation also linearly correlated well with the ISF, which means that increasing the ISF may lead to variability in surface runoff generation. For the grid cells with ISF < 6%, the annual surface runoff and the variation of daily surface runoff did not exhibit apparent linear correlations with the ISF. Therefore, an ISF of 6% may be a potential threshold for detecting urban growth effects on surface runoff. When the ISF is beyond this threshold, the increase of ISF will not only affect the magnitude of surface runoff but will also promote the dispersion of daily surface runoff.

4.4. Influence of ISA under historical rainstorm events

To identify potential flooding consequences of urban growth, four typical rainstorm events were selected from the VIC simulations regarding the "Urban" and the "No-urban" scenarios. The four rainstorm events were distributed in different decades with one-day spatial mean rainfall ranging from 62 to 118 mm (Table 3). As shown in Fig. 10, the spatial patterns of rainfall in the four events were quite different, however, their surface runoff generation was consistently concentrated in the Core-Zone and the Extended-Zone. For example, the rain event of July 6, 1998, focused on the west part of Beijing, departing from the city center, however the potential flooding area with devastating consequence (surface runoff > 50 mm) mainly spread over the Core-Zone and the Extended-Zone, and the surface runoff depth in the Core-Zone was over 80 mm for the event. If the urban growth was removed in the simulation (i.e., the "No-urban" scenario), however, the potential flooding area was substantially reduced and was instead concentrated in the Core-Zone and the rainstorm center areas.

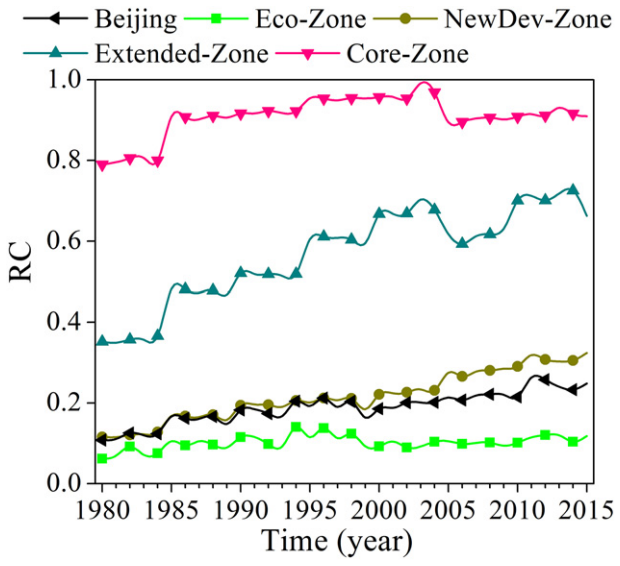

Fig. 7. Surface runoff coefficient (RC) of Beijing and the four zones in Beijing during 1980–2015.

We highlight the July 21, 2012, rainstorm event. The mean rainfall was approximately 118 mm in this event, which caused a surface runoff yield of 32.5 mm across Beijing. Particularly, the Core-Zone and the Extended-Zone had the largest surface runoff yields of 156.3 and 122.8 mm, respectively. The potential flooding area with devastating consequence was approximately 3207.7 km^2, extending to a part of the NewDev-Zone. For the "No-urban" scenario, the surface runoff yield was approximately 17.1 mm, which means that urban growth caused a 90.6% increase in surface runoff. Moreover, the potential flooding area was only approximately 887.8 km^2 and was concentrated in the Core-Zone and a part of the Extended-Zone.

The four events showed different surface runoff generation responses to urban growth and precipitation (Table 3). The difference in the surface runoff yield from the "Urban" and "No-urban" scenario was approximately 18.5% for the whole of Beijing in the August 25, 1985 event, however, the difference was up to 90.6% in the July 21, 2012 event. Thus, the potential flooding risk shows a significant correlation with urban growth. Moreover, the four zones in Beijing demonstrated an uneven response. The Extended-Zone and the NewDev-Zone show the largest increase in surface runoff yield, from 30 to 40% (in the August 25, 1985 event) to approximately or over 100% (in the July 21, 2012 event), relative to the scenario of "No-urban" growth, as these two zones have had rapid urban expansion.

We calculated the sensitivity coefficient S_c by taking the surface runoff from the Aug 25, 1985 event as the reference, and averaged the S_c regarding the other three events. Despite the uneven spatial distribution of precipitation, the averaged sensitivity coefficient S_c of surface runoff

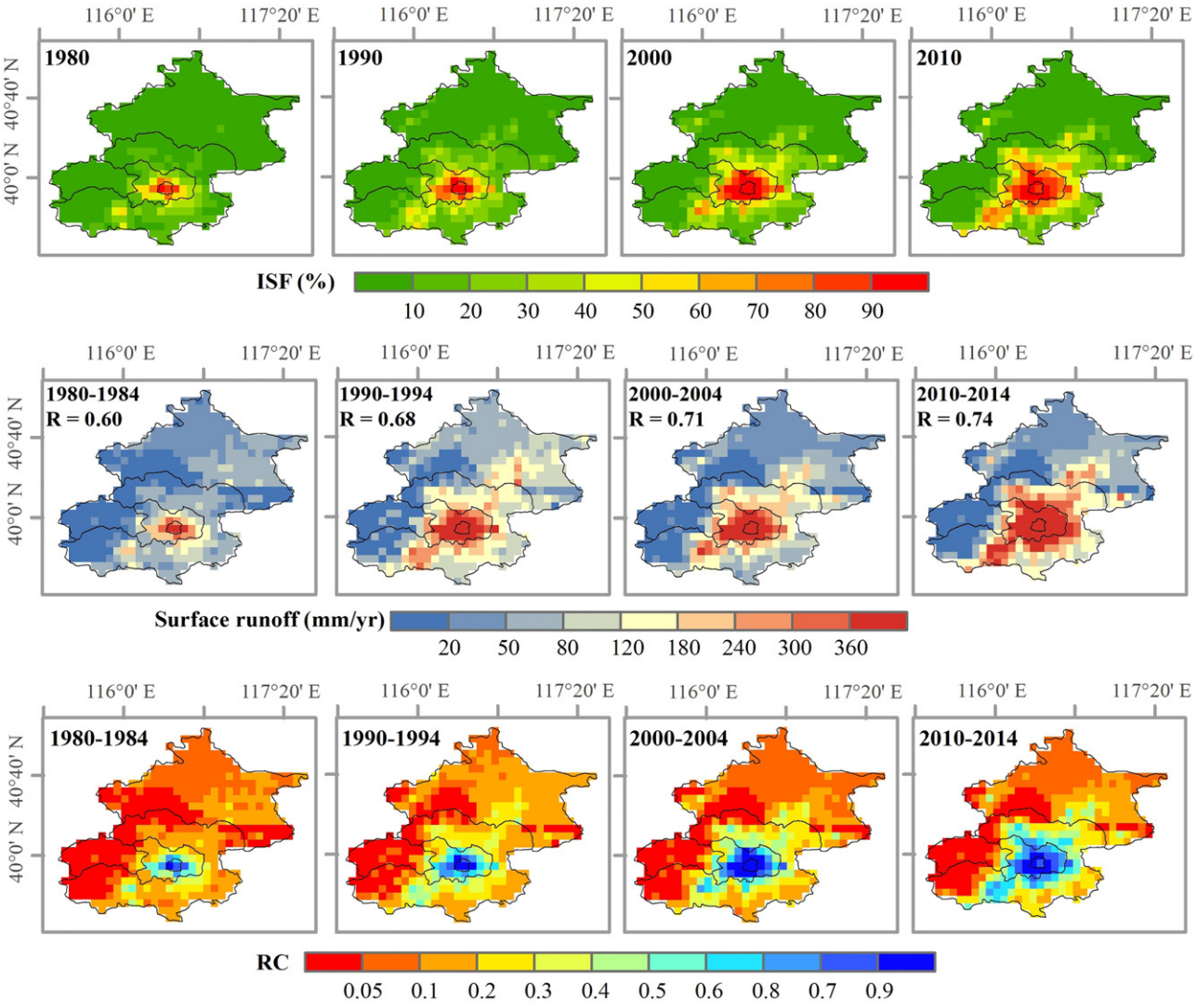

Fig. 8. The spatial distribution of ISF (top), surface runoff (middle), and RC (bottom) in Beijing. The time from left to right corresponds to the period of 1980–1984, 1990–1994, 2000–2004, and 2010–2014. The term of *R* in the middle plots is the correlation coefficient between the surface runoff and the associated ISF.

to precipitation was 0.97, and the S_c to ISF was up to 0.63. So the increased ISA dramatically enhanced the potential flooding risk, despite the dominant contribution of the rainstorm.

5. Discussion

5.1. Urban growth and surface runoff yield

This study captures the changes in ISF and the associated surface runoff in Beijing based on remote sensing data and VIC modeling. The overall ISF in Beijing increased by 13.49% during the period of 1980–2015, recording the urban growth in northeast-southwest directions from the Core-Zone. The urban area was mostly transformed from cropland. The ISAs estimated in this study is different from the results in Li et al. (2015), which reported that the area increased from approximately 745.92 km^2 to 2670.83 km^2 in the 1984–2013 period. This difference was partly attributable to the definition of an ISA. In the study by Li et al. (2015), the ISA did not include villages and related construction areas. Moreover, the satellite data used in Li et al. (2015) did not cover the entire area of Beijing and a small part was neglected. Xiang

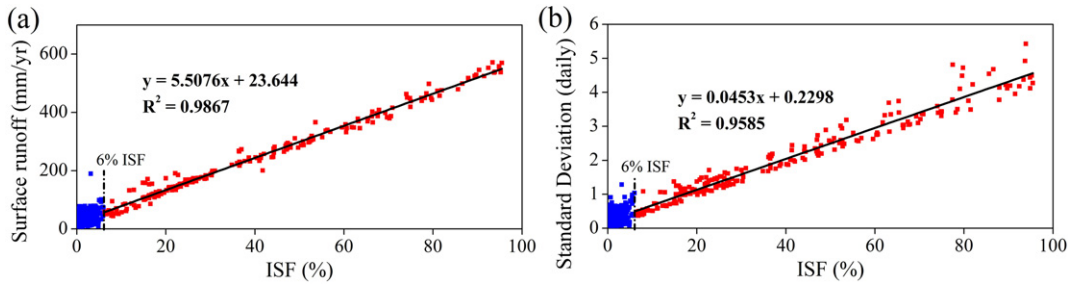

Fig. 9. The relationship of surface runoff and ISF for current conditions (2010–2014): (a) Annual average surface runoff; (b) standard deviation of daily surface runoff.

Table 3
Historical rainstorm data and surface runoff results.

Event date		Core-Zone	Expanded-Zone	NewDev-Zone	Eco-Zone	Beijing
Aug 25, 1985	Rainfall	101.0	105.1	79.7	81.9	82.9
	Surface runoff (Urban)	92.7	50.3	13.5	14.1	17.3
	Surface runoff (No-urban)	81.9	36.7	10.3	13.4	14.6
	Difference	13.2%	37.1%	30.1%	5.2%	18.5%
Jul 06, 1998	Rainfall	89.3	98.6	89.0	94.7	92.7
	Surface runoff (Urban)	85.5	59.0	19.0	13.4	19.6
	Surface runoff (No-urban)	72.0	35.0	11.8	10.6	13.4
	Difference	18.6%	68.6%	61.9%	26.4%	46.3%
Jul 23, 2005	Rainfall	65.5	68.5	74.2	52.5	62.1
	Surface runoff (Urban)	59.5	40.7	18.7	5.4	13.6
	Surface runoff (No-urban)	52.8	23.0	8.4	4.3	7.7
	Difference	12.5%	80.0%	122.6%	25.6%	76.6%
Jul 21, 2012	Rainfall	169.4	178.0	138.4	94.4	118.1
	Surface runoff (Urban)	156.3	122.8	40.4	12.2	32.5
	Surface runoff (No-urban)	136.9	62.4	17.0	8.8	17.1
	Difference	14.2%	96.8%	137.6%	39.8%	90.6%

et al. (2018) also derived the ISA for Beijing and the size is consistent with our study, indicating the reliability of the ISA estimation in this study.

After quantifying the urban growth, we explored the response of surface runoff. Urban growth caused a doubling in the annual RC for the whole of Beijing (from 0.12 to 0.25). The Extended-Zone and the NewDev-Zone showed the largest increases of surface runoff yield due to their dramatic increases in ISAs. Moreover, urban growth led to a >90% increase in surface runoff for the same level of storm event of July 21, 2012. Thus, the progress of urbanization in Beijing has obviously expanded the potential flooding risk.

These points have also been partly documented by other studies in Beijing. The urban commercial district in the Extended-Zone is susceptible to the highest potential flooding risk, especially for the total and the peak runoff depth (Yao et al., 2017; Yao et al., 2018). Y. Zhang et al. (2018) focused on a small catchment in Beijing and indicated that the extreme high flow depth has increased from 0.6% to 10.5% due to the increasing ISA. Jing et al. (2014) found that the flooding-affected area appeared a spatial expansion during the years of 1981–2011, which was primarily contributed to by the built-up area. These studies revealed the increasing potential of flooding risk in small catchment areas of Beijing. Our study has the advantages of

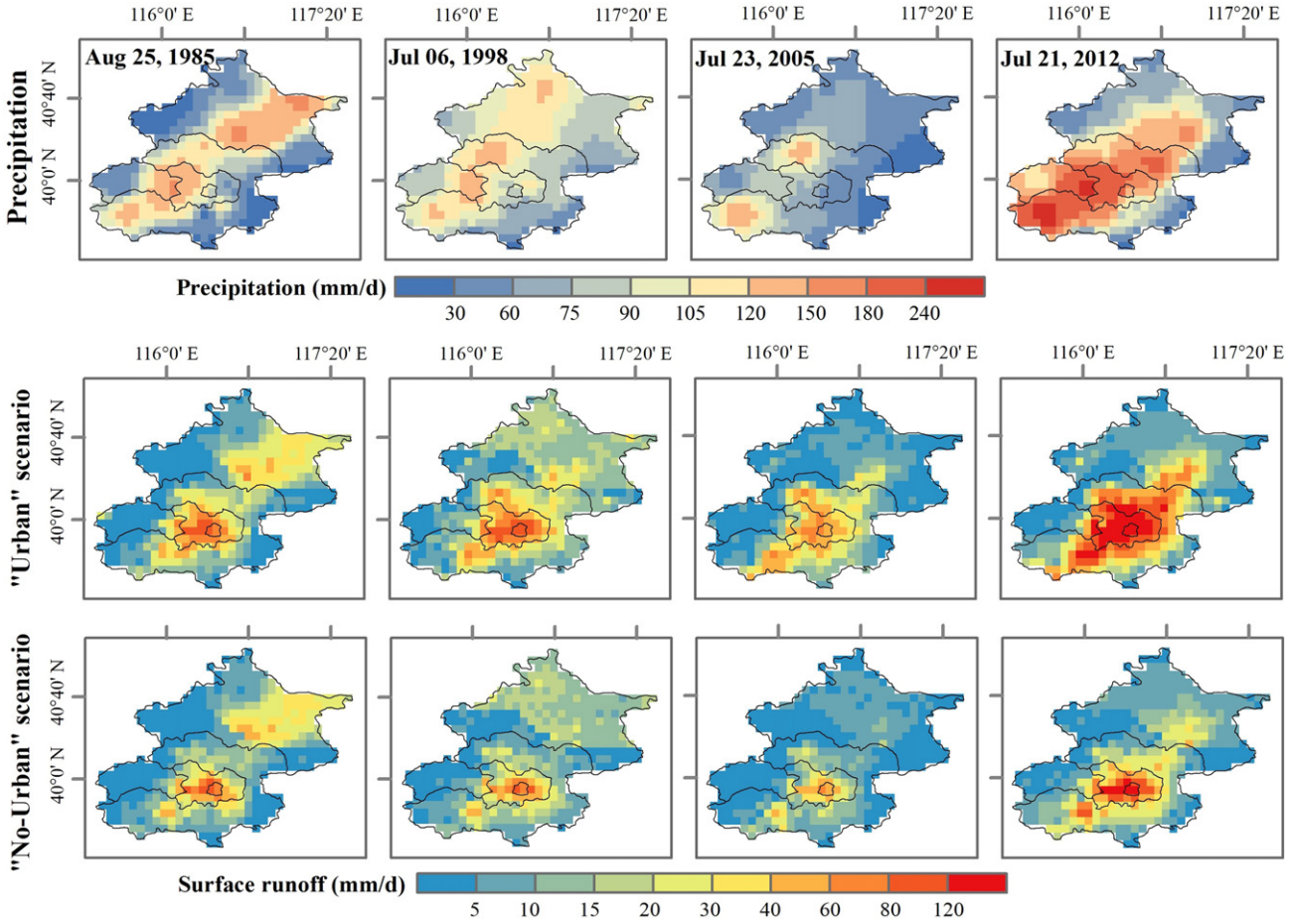

Fig. 10. Precipitation (top) and surface runoff distribution for the "Urban" (middle) and "No-urban" (bottom) scenarios under historical rainstorm events.

mapping the long-term dynamics of ISA throughout Beijing and quantifying the contribution of urban growth to the potential flooding risk.

Beijing is not alone with respect to urban growth and the associated hydrological response. Table 4 summaries seven relevant past studies for different regions and climate zones. According to these studies, urban growth leads to an increase in surface runoff (Zhou et al., 2013), high-flow frequency, and flow variability (Yang et al., 2010), which become severe in extreme weather events (W. Zhang et al., 2018; Zope et al., 2016). And Increases in ISA for rural catchments may have greater impact on floods than that for an existing urban area (Du et al., 2012; Miller et al., 2014). The magnitude of the increase may vary, partly depending on the climate condition, the progress of urbanization, and the adopted spatial and temporal scales. However, Beijing is a typical fast-growing megacity with a high-density population, and its potential flooding risk is worthy of attention due to its dramatic surface runoff increase in the period of 1980–2015.

5.2. Implications for the sponge city construction

The July 21, 2012 flooding disaster in Beijing raised considerable attention towards the green urban development and sponge city as a significant national strategy in China (Chan et al., 2018). The concept of a sponge city is to increase the management and storage capacity of rainwater in urban areas by constructing sponge measures for stormwater infiltration, retention, storage, purification, utilization, and drainage (Xia et al., 2017). For example, the use of permeable pavements should gradually spread to replace the traditional ISA for source control of runoff yield in extreme weather events (Y. Xu et al., 2018).

The results from this study may have implications for the sponge city construction. The ISA maps from remote sensing techniques illustrated the effectiveness in monitoring the urban growth, and the maps can serve as basic information for the design of a sponge city (Xia et al., 2017; Z. Xu et al., 2018). Specifically, the sponge measures should focus on regions prone to flooding and waterlogging, especially the Extended-Zone and the NewDev-Zone. Moreover, this study suggests that urban growth may not have obvious effects on surface runoff until the ISF is up to 6% in Beijing. With every 1% increase in the ISF exceeding this threshold, annual surface runoff is likely to increase by 5.51 mm/year with increasing temporal variability. This effect is primarily determined by regional climatic conditions. Therefore, areas with an ISF > 6% should be of high concern for the construction of sponge measures. Furthermore, the increasing potential flooding risk demonstrated in this study implies that the capability of real-time urban monitoring, hydrological forecasting, and emergency response programs should be strengthened to facilitate the management of future extreme weather events (Y. Zhang et al., 2018).

5.3. Limitations

This study has limitations in the ISA extraction and the hydrological modeling that may have induced potential uncertainties in the flood risk analysis for Beijing. First, the ISA extraction is sensitive to the data quality of the remote sensing images and the training samples in the CART algorithm. Our research covered three sensors (MSS, TM, and OLI), which may lead to slight differences in radiation, especially for the MSS sensor with a spatial resolution of 78 m in 1980. The training samples were manually selected by visual recognition, which also introduced uncertainties in the ISA extraction.

Second, the ISA in the VIC modeling was assumed as an effective impervious area onto which rainfall can directly convert to surface runoff. This assumption likely overestimates the surface runoff yield, because some roads and squares are actually permeable or partly permeable, and a certain portion of water from rainfall can be retained and is subsequently lost by evaporation even when rain falls on ISAs. Third, this study does not consider the connectivity of pervious surface and impervious surface. Actually, the two types of land cover are connected, like a mosaic. The surface runoff from ISAs can flow though the ISA and be detained by the neighboring pervious surface areas (e.g., grass), which allows the water to evaporate and infiltrate into the soil profile. Therefore, neglecting the connectivity may also induce overestimation of surface runoff yield to some degree (Schueler et al., 2009). Fourth, this study did not consider the runoff routing in the drainage system. The

Table 4
Summary of some relevant past works, for the assessment of ISA (Urban area) growth and its impact on regional (watershed) hydrology (the current paper is added for completeness).

Study region	Climate zone	Study period	ISF increase	Key result	Reference
White River (Indiana): 16 watersheds	Humid continental	1980–2003	0.80%	(1) Simulated high-flow increased by19% in frequency and by 12% in flow variability (2) 3%–5% ISA in a watershed is the detectable threshold	(Yang et al., 2010)
Qinhuai watershed (China)	Temperate monsoon	1988–2009	17.00%	(1) Slightly increases in mean annual runoff, dry year more obvious than wet year (2) The daily peak discharge of eight floods increased from 2.3% to 13.9% (3) The peak discharge and flood volume showed linear relationships with ISA	(Du et al., 2012)
Swindon (UK): 2 catchments	Temperate marine	1960–2010	33.00%	(1) Flood duration reduced by over 50%, peak flow increased by over 400% (2) Increases in ISA for rural catchments have greater impact on floods than that for an existing urban area	(Miller et al., 2014)
Houston	Subtropical monsoon-humid	(25–30)-08-2017	–	(1) Urbanization exacerbated both the flood response and the total rainfall (2) The probability of such extreme flood events increased on average by about 21 times in the period 25–30 August 2017 because of urbanization	(W. Zhang et al., 2018)
The United States	Various	2001–2011	0.22%	(1) Urban sprawl spread to suburban areas resulted in more medium and very high runoff counties (2) Ten states with top normalized average annual runoff depth value in 2011 were mainly influenced by high increases in urban land	(Chen et al., 2017)
Yangtze River Delta (China)	Subtropical monsoon	1985–2008	4.90%	(1) Surface runoff increased by 11.3%, and baseflow declined by 11.2% (2) The simulated peak discharge increased 1.6–4.3% and flood volume increased 0.7–2.3%	(Zhou et al., 2013)
Mumbai (India): Oshiwara River Basin	Tropical monsoon	1966–2009	13.79%	(1) Peak runoff increased by10.4%, runoff volume increased by 12.2% (2) The flood inundation area increased by 6.04% (3) The total flood hazard area is increased by 22.27%	(Zope et al., 2016)
Beijing (China)	Temperate monsoon	1980–2015	13.49%	(1) Surface runoff increased by 89.7% (i.e., the trend is 1.85 mm/year), and the simulated RC in 2010 increased by 0.13 compared to 1980 (2) 6% ISA in Beijing is the detectable threshold (3) Sensitivity coefficients of surface runoff to precipitation and ISA are 0.97 and 0.63, respectively	This study

drainage system in Beijing is complex as it was designed by different departments, and data regarding the drainage system are difficult to obtain. Therefore, the hydrological effect modeling for urban growth holds substantial uncertainties, and this study highlighted the potential flooding risk rather than actual flooding conditions.

6. Conclusions

This study characterized a 36-year change in the ISA in Beijing using Landsat data and identified the response of potential flooding risk to the urban growth based on a land-surface hydrological modeling technique (i.e., VIC). The VIC modeling features the incorporation of dynamic land cover changes (from multiple satellite remote sensing data) thereby reflecting the effect of the increased ISA. According to the model evaluation, the VIC modeling had an acceptable performance in reproducing streamflow observations ($R > 0.8$, $NSE > 0.4$). Based on the ISA extraction and hydrological modeling, this study achieved a few interesting conclusions:

(1) The ISA in Beijing increased from 1448.16 km^2 (ISF = 8.73%) to 3685.92 km^2 (ISF = 22.22%) during the period of 1980–2015, which was mainly due to land being transformed from cropland. The current distribution of the ISA represents the northeast-southwest urban growth pattern. Moreover, the urban growth is primarily concentrated in the Extended-Zone and the NewDev-Zone, with ISF increases of 33% and 21%, respectively.
(2) The urban dynamics obviously causes elevated runoff yields and RCs across Beijing. In the Extended-Zone and the NewDev-Zone, especially, the runoff yield increased at rates of 5.50 mm/year and 3.04 mm/year, respectively. The spatial distributions of the runoff yield and the RC were consistent with the ISA, indicating the considerable contribution of urban growth to the potential for flooding.
(3) An ISF threshold of approximately 6% is indicated for Beijing, above which urban growth is likely to promote runoff generation at a rate of 5.51 mm/year along with each 1% increase in the ISF, and below which the impact of urban growth was not linearly correlated with runoff yield. Moreover, the zones with a high ISF (>the threshold) in Beijing also have large variations in daily runoff generation, indicating the complexity of flood forecasting.
(4) The progress of urban growth increases the potential risk of devastating flooding under historical rainstorm event conditions. Despite the spatial variability of rainfall events, the devastating potential flooding risk is concentrated on the Core-Zone and the Extended-Zone, however, the expanding potential flooding risk is distributed in the Extended-Zone and the NewDev-Zone.

This study has limitations regarding the runoff generation on the ISA, the runoff routing through ISAs, and the drainage system. These limitations may have led to overestimations of the runoff yield and the flood risk for Beijing. Despite the mentioned limitations and uncertainties, this study characterized a 36-year ISA change in Beijing and provides an evaluation of the potential flooding risk and the contribution of urban growth during the period of 1980–2015. This provides a useful reference for urban planning and sponge city construction in China and worldwide. To obtain more detailed information regarding land surface properties and to consider the water flux interaction between adjacent grid cells, future studies can be dedicated to developing finer-resolution modeling (e.g., <1 km).

Declaration of competing interest

The authors declare that they have no known competing financial interests or personal relationships that could have appeared to influence the work reported in this paper.

Acknowledgments

This study was supported by grants from the National Key Research and Development Program of China (No. 2016YFA0600103, 2016YFC0401404) and the National Natural Science Foundation of China (No. 41971030).

References

AHR, 2016. Hydrological data of Haihe river basin. Annual Hydrological Report for the P.R. China. Bureau of Hydrology, Ministry of Water Resources.
Banskota, A., Kayastha, N., Falkowski, M.J., Wulder, M.A., Froese, R.E., White, J.C., 2014. Forest monitoring using Landsat time series data: a review. Can. J. Remote. Sens. 40, 362–384.
Bellu, A., Sanches Fernandes, L.F., Cortes, R.M.V., Pacheco, F.A.L., 2016. A framework model for the dimensioning and allocation of a detention basin system: the case of a flood-prone mountainous watershed. J. Hydrol. 533, 567–580.
Beven, K., 1979. A sensitivity analysis of the Penman-Monteith actual evapotranspiration estimates. J. Hydrol. 44, 169–190.
Caldas, A., Pissarra, T., Costa, R., Neto, F., Zanata, M., Parahyba, R., et al., 2018. Flood vulnerability, environmental land use conflicts, and conservation of soil and water: a study in the Batatais SP Municipality, Brazil. Water 10.
Chan, F.K.S., Griffiths, J.A., Higgitt, D., Xu, S., Zhu, F., Tang, Y.-T., et al., 2018. "Sponge City" in China—a breakthrough of planning and flood risk management in the urban context. Land Use Policy 76, 772–778.
Chen, J., Theller, L., Gitau, M.W., Engel, B.A., Harbor, J.M., 2017. Urbanization impacts on surface runoff of the contiguous United States. J. Environ. Manag. 187, 470–481.
Cuo, L., Zhang, Y., Gao, Y., Hao, Z., Cairang, L., 2013. The impacts of climate change and land cover/use transition on the hydrology in the upper Yellow River Basin, China. J. Hydrol. 502, 37–52.
Dai, Y., Shangguan, W., Duan, Q., Liu, B., Fu, S., Niu, G., 2013. Development of a China dataset of soil hydraulic parameters using pedotransfer functions for land surface modeling. J. Hydrometeorol. 14, 869–887.
Du, J., Qian, L., Rui, H., Zuo, T., Zheng, D., Xu, Y., et al., 2012. Assessing the effects of urbanization on annual runoff and flood events using an integrated hydrological modeling system for Qinhuai River basin, China. J. Hydrol. 464–465, 127–139.
Fletcher, T.D., Andrieu, H., Hamel, P., 2013. Understanding, management and modelling of urban hydrology and its consequences for receiving waters: a state of the art. Adv. Water Resour. 51, 261–279.
Gong, P., Li, X., Zhang, W., 2019. 40-year (1978–2017) human settlement changes in China reflected by impervious surfaces from satellite remote sensing. Science Bulletin 64, 756–763.
Hao, L., Huang, X., Qin, M., Liu, Y., Li, W., Sun, G., 2018. Ecohydrological processes explain urban dry island effects in a wet region, southern China. Water Resour. Res. 54, 6757–6771.
Jha, A.K., Bloch, R., Lamond, J., 2012. Cities and Flooding: A Guide to Integrated Urban Flood Risk Management for the 21st Century. World Bank Publications, Washington D C.
Jia, S., Li, Y., Lu, A., Liu, W., Zhu, W., Yan, J., et al., 2019. City storm-flood events in China, 1984–2015. International Journal of Water Resources Development 35, 605–618.
Jiang, Y., Zevenbergen, C., Ma, Y., 2018. Urban pluvial flooding and stormwater management: a contemporary review of China's challenges and "sponge cities" strategy. Environ. Sci. Pol. 80, 132–143.
Jing, Z., Yu, K., Li, D., 2014. Spatial characteristics of local floods in Beijing urban area. Urban Water J. 11, 557–572.
Konrad, C.P., Booth, D.B., 2005. Hydrologic changes in urban streams and their ecological significance. Am. Fish. Soc. Symp. 47, 157–177.
Li, X., Gong, P., Liang, L., 2015. A 30-year (1984–2013) record of annual urban dynamics of Beijing City derived from Landsat data. Remote Sens. Environ. 166, 78–90.
Liang, X., Xie, Z., 2001. A new surface runoff parameterization with subgrid-scale soil heterogeneity for land surface models. Adv. Water Resour. 24, 1173–1193.
Liang, X., Lettenmaier, D.P., Wood, E.F., Burges, S.J., 1994. A simple hydrologically based model of land surface water and energy fluxes for general circulation models. Journal of Geographical Research 99, 14415–14428.
Liang, X., Wood, E.F., Lettenmaier, D.P., 1996. Surface soil moisture parameterization of the VIC-2L model: evaluation and modification. Glob. Planet. Chang. 13, 195–206.
Liang, S., Xiang, Z., Liu, S., Yuan, W., Xiao, C., Xiao, Z., et al., 2013. A long-term Global LAnd Surface Satellite (GLASS) data-set for environmental studies. International Journal of Digital Earth 6, 5–33.
Liang, S., Zhang, X., Xiao, Z., Jie, C., Qiang, L., Xiang, Z., 2014. Global LAnd Surface Satellite (GLASS) Products. Springer International Publishing.
Liu, J., Liu, M., Zhuang, D., Zhang, Z., Deng, X., 2003. Study on spatial pattern of land-use change in China during 1995—2000. Science China-earth Sciences 46, 373–384.
Liu, J., Zhang, Z., Xu, X., Kuang, W., Zhou, W., Zhang, S., et al., 2010. Spatial patterns and driving forces of land use change in China during the early 21st century. J. Geogr. Sci. 20, 483–494.
Liu, Z., Li, Y., Peng, J., 2011. Progress and perspective of the research on hydrological effects of urban impervious surface on water environment. Prog. Geogr. 30, 275–281.
Liu, J., Kuang, W., Zhang, Z., Xu, X., Qin, Y., Ning, J., et al., 2014. Spatiotemporal characteristics, patterns, and causes of land-use changes in China since the late 1980s. J. Geogr. Sci. 24, 195–210.
Lohmann, D., Lettenmaier, D.P., Liang, X., Wood, E.F., Boone, A., Chang, S., et al., 1998. The Project for Intercomparison of Land-surface Parameterization Schemes (PILPS) phase 2(c) Red–Arkansas River basin experiment. Glob. Planet. Chang. 19, 161–179.

Miguel, C., Duong, N., Chinh, T., Luisa, Y., Jefferson, F., 2014. Mapping urban transitions using multi-temporal Landsat and DMSP-OLS night-time lights imagery of the Red River Delta in Vietnam. Land 3, 148–166.
Miller, J.D., Kim, H., Kjeldsen, T.R., Packman, J., Grebby, S., Dearden, R., 2014. Assessing the impact of urbanization on storm runoff in a peri-urban catchment using historical change in impervious cover. J. Hydrol. 515, 59–70.
Milly, P.C.D., Betancourt, J., Falkenmark, M., Hirsch, R.M., Kundzewicz, Z.W., Lettenmaier, D.P., et al., 2008. Stationarity is dead: whither water management? Science 319, 573–574.
Nash, J.E., Sutcliffe, J.V., 1970. River flow forecasting through conceptual models part I–a discussion of principles. J. Hydrol. 10, 282–290.
Nijssen, B., Schnur, R., Lettenmaier, D.P., 2001. Global retrospective estimation of soil moisture using the variable infiltration capacity land surface model, 1980–93. J. Clim. 14, 1790–1808.
Nijssen, B., Bowling, L.C., Lettenmaier, D.P., Clark, D.B., El Maayar, M., Essery, R., et al., 2003. Simulation of high latitude hydrological processes in the Torne–Kalix basin: PILPS Phase 2(e). Glob. Planet. Chang. 38, 31–53.
Olang, L.O., Fürst, J., 2011. Effects of land cover change on flood peak discharges and runoff volumes: model estimates for the Nyando River Basin, Kenya. Hydrol. Process. 25, 80–89.
Pumo, D., Arnone, E., Francipane, A., Caracciolo, D., Noto, L.V., 2017. Potential implications of climate change and urbanization on watershed hydrology. J. Hydrol. 554, 80–99.
Qi, L., Yue, C., 2011. Classification of remote sensing image based on CART decision tree method. Forestry survey planning 36, 62–66.
Rose, S., Peters, N.E., 2001. Effects of urbanization on streamflow in the Atlanta area (Georgia, USA): a comparative hydrological approach. Hydrol. Process. 15, 1441–1457.
Salvadore, E., Bronders, J., Batelaan, O., 2015. Hydrological modelling of urbanized catchments: a review and future directions. J. Hydrol. 529, 62–81.
Sanches Fernandes, L.F., Terêncio, D.P.S., Pacheco, F.A.L., 2015. Rainwater harvesting systems for low demanding applications. Sci. Total Environ. 529, 91–100.
Schueler, T.R., Fraley-mcneal, L., C, K., 2009. Is impervious cover still important: review of recent research. J. Hydrol. Eng. 14, 309–315.
Sexton, J.O., Song, X.-P., Huang, C., Channan, S., Baker, M.E., Townshend, J.R., 2013. Urban growth of the Washington, D.C.–Baltimore, MD metropolitan region from 1984 to 2010 by annual, Landsat-based estimates of impervious cover. Remote Sens. Environ. 129, 42–53.
Statistics, 2018. Beijing Statistical Yearbook-Beijing. Municipal Bureau of Statistics, Survey Office of the Bureau of Statistics in Beijing.
Terêncio, D.P.S., Sanches Fernandes, L.F., Cortes, R.M.V., Pacheco, F.A.L., 2017. Improved framework model to allocate optimal rainwater harvesting sites in small watersheds for agro-forestry uses. J. Hydrol. 550, 318–330.
UN, 2018. United Nations population division world urbanization prospects: the 2018 revision. https://population.un.org/wup/, Accessed date: 13 July 2019.
Wei, S., Dai, Y., Liu, B., Zhu, A., Duan, Q., Wu, L., et al., 2013. A China data set of soil properties for land surface modeling. Journal of Advances in Modeling Earth Systems 5, 212–224.
Wu, J.S., Pan, J.Y., Peng, J., 2012. Classification of remote sensing image land use based on QUEST decision tree — a case study of Lijiang city, Yunnan province. Geogr. Res. 31, 1973–1980.
Xia, J., Zhang, Y., Xiong, L., He, S., Wang, L., Yu, Z., 2017. Opportunities and challenges of the Sponge City construction related to urban water issues in China. Science China Earth Sciences 60, 652–658.
Xiang, C., Zhu, X., Hu, D., Qiao, K., Chen, S., 2018. Monitoring of the impervious surface with multi-resource remote sensing images in Beijing-Tianjin-Tangshan urban agglomeration in the past two decades. Journal of earth information science 20, 684–693.
Xiao, Z., Liang, S., Wang, J., Chen, P., Yin, X., Zhang, L., et al., 2014. Use of general regression neural networks for generating the GLASS leaf area index product from time-series MODIS surface reflectance. IEEE Transactions on Geoscience & Remote Sensing 52, 209–223.
Xiao, Z., Liang, S., Wang, J., Xiang, Y., Zhao, X., Song, J., 2016. Long-time-series global land surface satellite leaf area index product derived from MODIS and AVHRR surface reflectance. IEEE Trans. Geosci. Remote Sens. 54, 5301–5318.
Xie, Z., Su, F., Xu, L., Zeng, Q., Zhenchun, H., Yufu, G., 2003. Applications of a surface runoff model with Horton and Dunne runoff for VIC. Adv. Atmos. Sci. 20, 165–172.
Xie, Z., Yuan, F., Duan, Q., Zheng, J., Liang, M., Chen, F., 2007. Regional parameter estimation of the VIC land surface model: methodology and application to river basins in China. J. Hydrometeorol. 8, 447–468.
Xie, X., Liang, S., Yao, Y., Jia, K., Meng, S., Li, J., 2015. Detection and attribution of changes in hydrological cycle over the Three-North region of China: climate change versus afforestation effect. Agric. For. Meteorol. 203, 74–87.
Xie, G., Yao, Y., Li, J., Yang, J., Bai, J., Ferguson, D.K., et al., 2019. Holocene climate, dynamic landscapes and environmentally driven changes in human living conditions in Beijing. Earth Sci. Rev. 191, 57–65.
Xu, Z., 2018. Influence of urbanization in Beijing on storm flood process and its numerical simulation. China Flood & Drought Management 2, 4.
Xu, Z., Cheng, T., Ren, M., 2017. Farewell to urban flooding: a brief discussion on the functions and features of Sponge City. China Flood & Drought Management 27, 64–66.
Xu, Y., Shen, S., Lai, Y., Zhou, A., 2018a. Design of Sponge City: lessons learnt from an ancient drainage system in Ganzhou, China. J. Hydrol. 563, 900–908.
Xu, Z., Cheng, T., Hong, S., Wang, L., 2018b. Review on applications of remote sensing in urban flood modeling. Chinese Science Press 63, 2156–2166.
Yang, G., Bowling, L.C., Cherkauer, K.A., Pijanowski, B.C., Niyogi, D., 2010. Hydroclimatic response of watersheds to urban intensity: an observational and modeling-based analysis for the White River Basin, Indiana. J. Hydrometeorol. 11, 122–138.
Yang, G., Bowling, L.C., Cherkauer, K.A., Pijanowski, B.C., 2011. The impact of urban development on hydrologic regime from catchment to basin scales. Landsc. Urban Plan. 103, 237–247.
Yang, P., Jin, J., Zhao, D., li, J., 2016. An urban vulnerability study based on historical flood data: a case study of Beijing. Sci. Geogr. Sin. 36, 733–741.
Yao, L., Chen, L., Wei, W., 2017. Exploring the linkage between urban flood risk and spatial patterns in small urbanized catchments of Beijing, China. Int. J. Environ. Res. Public Health 14, 239.
Yao, L., Wei, W., Yu, Y., Xiao, J., Chen, L., 2018. Rainfall-runoff risk characteristics of urban function zones in Beijing using the SCS-CN model. J. Geogr. Sci. 28, 656–668.
Zhang, L., Qian, N., 2015. Two improvements on CART decision tree and its application. Computer Engineering & Design 36, 1209–1213.
Zhang, W., Villarini, G., Vecchi, G.A., Smith, J.A., 2018a. Urbanization exacerbated the rainfall and flooding caused by hurricane Harvey in Houston. Nature 563, 384–388.
Zhang, Y., Xia, J., Yu, J., Randall, M., Zhang, Y., Zhao, T., et al., 2018b. Simulation and assessment of urbanization impacts on runoff metrics: insights from landuse changes. J. Hydrol. 560, 247–258.
Zhou, F., Xu, Y., Chen, Y., Xu, C.Y., Gao, Y., Du, J., 2013. Hydrological response to urbanization at different spatio-temporal scales simulated by coupling of CLUE-S and the SWAT model in the Yangtze River Delta region. J. Hydrol. 485, 113–125.
Zhu, B., Xie, X., Lu, C., Meng, S., Yao, Y., Wang, Y., 2019. Toward high-spatial resolution hydrological modeling for China: calibrating the VIC model. Hydrol. Earth Syst. Sci. Discuss. 1–43.
Zope, P.E., Eldho, T.I., Jothiprakash, V., 2016. Impacts of land use–land cover change and urbanization on flooding: a case study of Oshiwara River Basin in Mumbai, India. Catena 145, 142–154.